REVIEW

An introductory review of the thermal structure of subduction zones: III. Comparison between models and observations

Peter E. van Keken* and Cian R. Wilson

*Correspondence: pvankeken@carnegiescience.edu
Earth and Planets Laboratory, Carnegie Institution for Science, 5241 Broad Branch Road, NW, Washington DC 20015, USA.
Full list of author information is available at the end of the article

Abstract

The thermal structure of subduction zones is fundamental to our understanding of the physical and chemical processes that occur at active convergent plate margins. These include magma generation and related arc volcanism, shallow and deep seismicity, and metamorphic reactions that can release fluids. Computational models can predict the thermal structure to great numerical precision when models are fully described but this does not guarantee accuracy or applicability. In a trio of companion papers the construction of thermal subduction zone models, their use in subduction zone studies, and their link to geophysical and geochemical observations are explored. In this last part we discuss how independent finite element approaches predict the thermal structure of the global subduction system and investigate how well these predictions correspond to geophysical, geochemical, and petrological observations.

Keywords

Geodynamics, Plate tectonics, Finite element methods, Subduction zone metamorphism, Arc volcanism

1 Introduction

This paper is a companion to van Keken and Wilson "An introductory review of the thermal structure of subduction zones: I–motivation and selected examples" (van Keken and Wilson, 2023, hereafter referred to as part I) and Wilson and van Keken "An introductory review of the thermal structure of subduction zones: II. Numerical approach and validation" (hereafter referred to as part II). A preprint to part II is available in the Supplementary Information.

Combined these articles provide an introduction to the use of thermal models and observational constraints to aid our understanding of the dynamics, structure, and evolution of subduction zones from a geophysical, geochemical, and petrological perspective. In Part I we provided the motivation for these studies, fundamental constraints on subduction zone geometry and thermal structure, along with a limited overview of existing thermal models. In Part II we provided a discussion of the use of the finite element method to discretize partial differential equations needed for subduction zone modeling, presented open-source software for their solution, and discussed validation & verification approaches. In this last part we will first show how various modeling approaches predict the thermal structure of the global subduction system using published compilations. We will then provide a broad comparison of model predictions to geophysical and geochemical observations to understand how well these models predict the thermal structure of subduction zones and where they fail.

Our approach will be similar to that in Part I and II – we strive to make this introduction accessible to advanced undergraduates, graduate students, and professionals from outside geodynamics. This will, hopefully, make the reader able to establish a fundamental understanding of what is required for numerical modeling of the thermal structure of subduction zones and how these models are used and evaluated using code intercomparisons and observations.

2 Comparison between different approaches to predict subduction zone thermal structure

We will first describe how various approaches used to model subduction zone thermal structure compare. These will be largely based on work introduced in part II. Model equations, nondimensionalization, geometrical assumptions, solution methods, etc. are fully described in section 2.3 therein.

We will show how different numerical approaches (TerraFERMA vs. Sepran) establish the numerical solution for the 56 global subduction zones from Syracuse et al. (2010) using the same model description (that is, identical geometry, subduction speed, boundary & initial conditions, and mantle wedge rheology). We will then turn to a more free-form exercise where we compare the 17 models of Wada and Wang (2009) to a similar selection of models from Syracuse et al. (2010). This second comparison will therefore show the differences that can be incurred when independent teams of researchers try to predict the thermal structure of subduction zones without explicit alignment of assumptions.

2.1 Corrections and clarifications regarding models from Syracuse et al. (2010)

In the Supplementary Information we have provided a full set of models that are similar to the D80 models in Syracuse et al. (2010) but have a number of corrections which were due to a small number of incorrect entries in input files (the infamous "user error" that is an unfortunate but common source for imprecise computations!) and a source code error in the trench-side boundary condition for some models. This last error had an impact for the affected subduction models particularly at shallow depths but was fixed before any of the computations in van Keken et al. (2011) or those in later publications were done. All other inconsistencies had only minor impact, yet we recommend using this updated data set instead of relying on the tables in the original paper. In the Supplementary Information we have provided an update to Table 2 from Syracuse et al. (2010) that specifies all corrections and clarifications made. We will refer to the updated set of models simply as "D80". A further typographical error occurred in Table 1 of Syracuse et al. (2010): the mantle thermal conductivity used in the modeling was 3.1 W/(m K) and not 2.5 W/(m K).

2.2 A few examples: Central Honshu, Alaska Peninsula, and Cascadia

In the next step in our exploration of how to validate and verify thermal modeling of subduction zones (as started in part II) we focus on the global compilation of models from Syracuse et al. (2010) and compare predictions made by TerraFERMA and Sepran. This allows us to investigate the differences in predictions from two fully

Figure 1 Comparison between TerraFERMA and Sepran predictions for the thermal structure of the models for Cascadia (row a), Alaska Peninsula (row b), and Central Honshu (row c) from Syracuse et al. (2010) with modifications as described in the text. In these models as in any other Sepran or TerraFERMA models presented in this paper we have added a posteriori an adiabat of 0.3°C/km (as in Syracuse et al., 2010). Column 1: Temperature as predicted by TerraFERMA. Slab top is indicated by the solid line and the slab Moho by the dashed line. Column 2: Temperature difference between predictions from TerraFERMA and Sepran. Slab top and Moho indicated as in column 1. Column 3: Comparison of the temperature at the slab top and slab Moho. Lines are from TerraFERMA (slab top solid lines, slab Moho dashed lines), open circles are from Sepran.

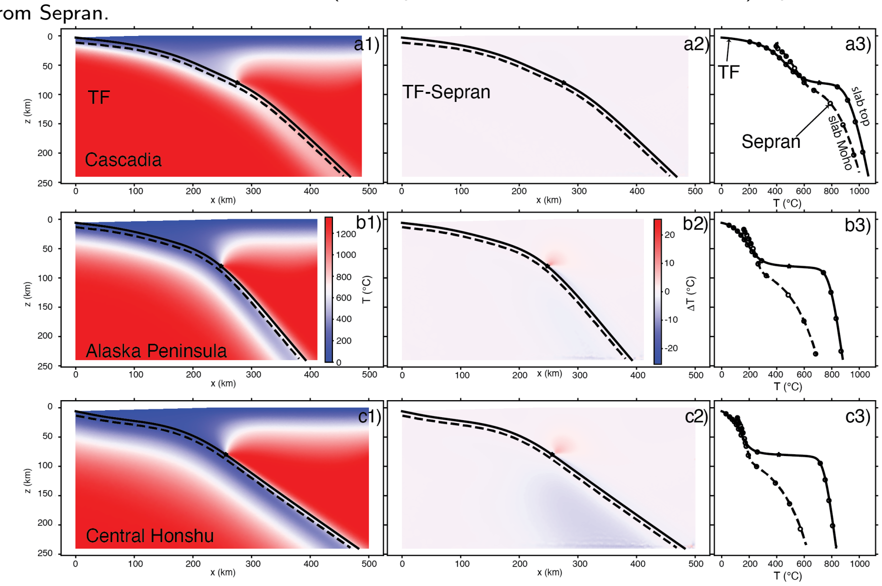

independent finite element approaches of models that are completely described in terms of geometry, boundary conditions, initial conditions, constitutive parameters, and age and speed of the incoming plate.

We use the model geometries from Syracuse et al. (2010) and make a few modifications in the following manner: i) instead of a mantle potential temperature of 1422°C we use a more moderate 1350°C; ii) instead of the GDH1 plate cooling model we use the halfspace cooling model; and iii) we cap the age of the incoming lithosphere at 100 Myr. We also find the velocity in the slab by solving the Stokes equation rather than prescribing it kinematically as in Syracuse et al. (2010). We will refer to this new set of models that still is closely based on the original D80 models from Syracuse et al. (2010) as "D80new."

To demonstrate the importance of the speed of the subduction and the age of the incoming plate (which makes up most of the thermal parameter Φ; see part I) we show three examples: a model for Central Honshu (or, perhaps better, southern Tohoku - fast subduction of old oceanic lithosphere); one for Alaska Peninsula (moderately fast subduction of intermediately aged oceanic lithosphere); and Cascadia (slow subduction of very young oceanic lithosphere). A complete comparison of all 56 subduction zones from Syracuse et al. (2010) under the modifications discussed above is in the Supplementary Information. All models are time-dependent. Total integration time for most models is 40 Myr which is sufficient for the slab to nearly reach a steady-state thermal structure (see Part II).

Figure 1 shows the temperature obtained by TerraFERMA for the three models, the differences with the Sepran results, and the slab top and slab Moho temperature profiles predicted by both approaches. Differences in predicted temperature along the slab top and Moho tend to be negligible. A temperature difference "bubble" shows up right above the coupling point similar to what was observed in the benchmark comparison shown in part II. There is also a minor difference in deep slab thermal structure predicted for Central Honshu which may be due to the high subduction speed here.

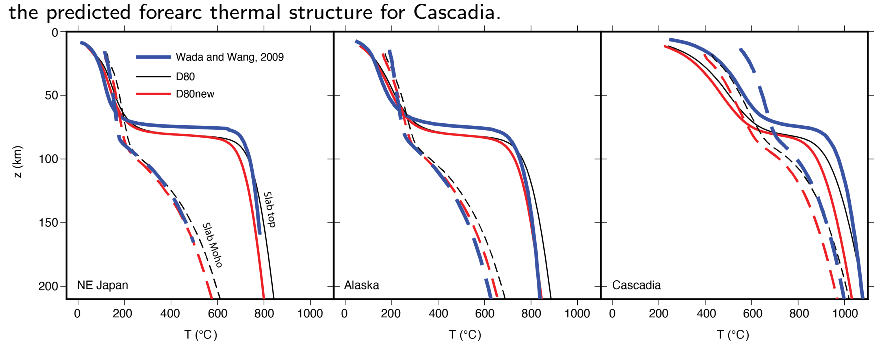

Figure 2 Comparison of slab top and slab Moho temperatures for a) NE Japan, b) Alaska, and c) Cascadia as predicted by three different approaches: 1) Updated D80 Sepran models from Syracuse et al. (2010) as discussed in text. 2) Sepran models following D80new description as discussed in section 2.2. 3) Fully independent models from Wada and Wang (2009). The models agree moderately well – main differences are due to the shallower decoupling depth d_c used in Wada and Wang (2009) and the difference in mantle temperature between the original D80 models and the new model set presented here. In addition the use of a younger age of the incoming lithosphere in Wada and Wang (2009) for Cascadia (8 Myr vs. 10 Myr) leads to a pronounced warming of the slab thermal structure – even minor differences in slab age have a strong influence in young subduction zones due the the change in thermal gradients in the shallow lithosphere. The Cascadia model from Wada and Wang (2009) is also warmer particularly at shallow depth because of the different treatment of modeling the effects of the thick sediment section which leads to a warmer initial thermal structure of the oceanic crust compared to the D80 model. Combined these different model assumptions cause a relatively significant difference in the predicted forearc thermal structure for Cascadia.

2.3 Importance of modeling assumptions

We now turn to the importance of the model assumptions that are made. While we have demonstrated that the solution of the governing differential equations by two independent finite element models leads to very similar temperature predictions for the same set of model assumptions, the differences caused by reasonable variations and uncertainties in those model assumptions are potentially large. In Table 1 we provide a good faith estimate of the potential thermal effect of several mechanisms that are not explicitly modeled in Syracuse et al. (2010). These estimates should not be taken overly seriously – they are loosely based on comparisons between models and observations and independent modeling published elsewhere (as discussed in section 3).

As we will see, important causes for these uncertainties are the simplification from the 3D time-dependent "real" subduction zones to those represented by quasi-steady-state 2D models. Further potentially important causes for uncertainty are in general the rheology of the mantle wedge, the strength of the seismogenic zone, other constitutive parameters, the parameterization of the decoupling zone between

Table 1 Estimates of thermal effects of processes not modeled in Syracuse et al. (2010)

Effect	Impact	Temperature difference
Primary		
melt migration	local	few 100°C
backarc spreading	local and shallow	few 100°C
time-dependence of forcing parameters	global	100–200°C
3D flow effects	global	100–200°C
rheology of the mantle wedge	global	??
variable radiogenic heating	local	∼50–100°C
decoupling-coupling transition	local	could be large locally
Secondary		
fluid flow in slab	local to shallow slab	10–50°C
shear heating	local to seismogenic zone	50–100°C
phase changes	local to shallow slab	50°C

the slab and mantle wedge, and the choice of d_c. More specifically these include the geometry of the subduction zone, the age and speed of the incoming plate, and whether models are steady state or evolved over a certain time interval.

In one example of a direct comparison between independent model approaches, Chen et al. (2019) reported differences in slab surface temperatures between Syracuse et al. (2010) and their models of only 20–60°C at 240 km depth. Another example is provided in Figure 2 that shows the slab top and oceanic Moho temperatures for three selected models used in section 2.2 similar to the N. Cascadia, Alaska, and NE Japan models from Wada and Wang (2009). See the caption for discussion. A full comparison between all 17 models of Wada and Wang (2009) and (closest) representatives thereof in D80 and D80new is provided in the Supplementary Information.

3 Comparison between model predictions and observations

We now turn to an evaluation of predictions from the thermal modeling discussed above in the context of geochemical and geophysical observations. It is certainly not expected that any given thermal model for a particular arc will confidently predict all local observations; nor can it be expected that global compilations predict global characteristics of geophysical or geochemical data bases. But it is of interest to investigate where the models seem to provide reasonable predictions and where they fail.

Before we embark on this journey it is useful to recap the features and limitations of the presented thermal models. To focus we will explore the updated D80 models. Important assumptions are that:

a) the slab geometry is based on a regional average of up to 500 km along-trench distance and is taken from the slab geometry models presented in Syracuse and Abers (2006);

b) forcing parameters such as the slab velocity and incoming plate age are assumed constant and the models have a fixed decoupling depth d_c=80 km;

c) the rheology of the wedge is assumed to be governed by dislocation creep in dry olivine;

d) the models ignore phase changes or the effects of fluid flow or magma migration;

e) the overriding lithosphere is cold and does not deform & the model geometry is fixed;

f) the models are time-dependent and evolved for ∼40 Myr causing the slab thermal structure to be in near steady state;

g) radiogenic heating is included in the continental crust of the overriding plate but shear heating and viscous dissipation are ignored;

h) the mantle potential temperature is assumed to be constant and is based on the value of 1422°C for the GDH1 plate model (Stein and Stein, 1992);

i) no individual adjustments to any subduction zone model are made to match local conditions except for ocean-ocean subduction (where the integration time may have been shortened to 20 Myr to avoid overthickening of the overriding lithosphere) and for Nankai (which has a geologically relevant young integration time of ∼20 Myr; Kimura et al., 2005).

In the updated set of D80 models the slab top temperatures tend to be slightly warmer than those in the original compilation due to some of the issues mentioned before. We have provided the below-arc slab-top temperatures (where we take the top of the slab to be the top of the sediments) in an update to part of the original Table 3 in Syracuse et al. (2010) and compared the older (and slightly incorrect values) with those from the D80 and D80new model updates. Any references to the thermal structure of the slab and wedge below are based on the updated D80 results.

3.1 Slab surface temperature: to melt the slab or not?

A number of geochemical studies provide constraints on the slab surface temperature below the arc. The comparison below shows some encouraging agreement between models and observations and hopefully will stimulate further interdisciplinary work.

An estimate of 700–900°C for slab-top temperatures below arcs globally was provided by Hermann and Spandler (2008). It is based on an experimental melting study of pelites and agrees well with the below-arc slab top temperature range in D80 of 762–964°C with an average of 841°C (1σ=48°C). Only six of the 56 subduction zones predict below-arc slab temperatures above 900°C. An experimental study on melting of radiolarian clay suggested that, depending on water content, the minimum slab surface temperature in the Lesser Antilles should be between 780–840°C (Skora and Blundy, 2010); the D80 models suggest a below-arc temperature of 803°C for the Northern Lesser Antilles and 848°C for the Southern Lesser Antilles. The updated model estimates also better explain the evidence for slab melting here (White et al., 2017). This should occur between 790–850°C according to melting experiments by Schmidt et al. (2004). Note that for this subduction zone, the lower contribution of slab melts that is expected due to the predicted lower temperature in Northern Lesser Antilles compared to that in the southern section was confirmed from a molybdenum isotopic study tracing subducted black shales (Freymuth et al., 2016).

Less impressive agreement was found for Eastern Banda. Lu-Hf-Zr isotopic observations, combined with experimental constraints on the disappearance of Zr, suggest the slab surface temperature below the arc should be near 925°C (Nebel et al., 2011). This is well above the D80 prediction of 864°C for this region and may potentially indicate mantle wedge flow around the edge of the subducting slab in this region. Such 3D toroidal flow is likely to increase the slab surface temperature locally as the warm asthenosphere can be advected more efficiently compared to that in a 2D flow geometry. Alternatively, the comparison is not optimal since it is at the strongly curved eastern terminus of the Indonesian arc which makes the 2D model predictions likely inaccurate for this arc (see the Discussion).

A relatively new slab geothermometer based on H_2O/Ce was introduced by Plank et al. (2009) who demonstrated a rapid increase in slab surface temperature obtained from sampling of volcanoes that trend away from the trench in Kamchatka. This is in good quantitative agreement with a selection of numerical models for this region. The authors acknowledged potential limitations in the applicability of this new thermometer particularly in their supplementary information, but it is nevertheless remarkable that a comparison between slab surface temperatures estimated from this thermometer and those obtained by Syracuse et al. (2010) provide good agreement (on average less than 50°C difference) for multiple arcs across nearly the full range of slab surface temperatures (see Figure 9 in Cooper et al., 2012). The strongest deviation is for Irazu (Costa Rica) which was modeled at the time with a nearly 200°C lower temperature than observed. The updated D80 model for Costa Rica closes the gap by 100°C; the remainder can potentially be explained by toroidal flow along the southern edge of this margin. In a related paper, Ruscitto et al. (2012) used magma volatile content to argue that slab dehydration occurs deeper in the mantle if the slab thermal parameter is larger which is in good quantitative agreement with thermal model predictions. Application of the H_2O/Ce thermometer suggested that the slab surface temperature below the Tonga arc matches the D80 model but the slab surface below the backarc appears to be warmer by about 100°C than the thermal model suggests (Caulfield et al., 2012). This difference again could potentially, again, be due to toroidal flow. Geochemical observations in the Lau Basin support such flow around the northern end of the Tonga subduction zone (Turner and Hawkesworth, 1998).

In a more qualitative fashion, evidence for melting of the subducted oceanic crust below arcs (Peacock et al., 1994) has been satisfactorily explained with models that take into account the temperature-dependence of olivine rheology (van Keken et al., 2002); in fact, at least the uppermost part of the oceanic crust is expected to experience hydrous melting when it gets into contact with the hot mantle wedge in all modeled subduction zones except Tonga (van Keken et al., 2011) assuming no major dehydration occurs beforehand. This is a concern in the very warm Cascadia subduction zone where the oceanic crust is predicted to dehydrate completely below the forearc (van Keken et al., 2011) suggesting that any fluids that trigger flux melting in this arc are not likely sourced from the descending oceanic crust. An elegant solution was provided by Walowski et al. (2015, 2016) who showed using hydrogen and boron isotopes that the source for fluids is from the hydrated uppermost mantle rather than from the oceanic crust. Thermal models show that final dehydration of the uppermost mantle indeed occurs below the arc (see Figure 3c in van Keken et al., 2011). The suggestion for crustal melting in the Cascadia subduction zone is supported by seismological observations of partially molten crust underneath Mount St. Helens (Crosbie et al., 2019). Independent work combining geochemical observations and thermal modeling also suggested the important role of serpentinite dehydration in triggering arc volcanism in Kamchatka (Konrad-Schmolke et al., 2016).

The Calabria/Aeolian arc is another example where evidence for slab melting is at odds with the modeled slab thermal structure. Zamboni et al. (2016) showed B-Be evidence for slab melting along the edges. The authors attribute this to 3D toroidal flow around the edges, which may also cause the strong along-arc geochemical variations. It is intriguing that this subduction zone with large thermal parameter (Φ=5600 km) can have similar geochemical characteristics as those of subduction zones with much smaller thermal parameter, such as Cascadia with Φ=150 km.

3.2 Primary arc magma formation in the hot mantle wedge

The thermal models can also be compared to geochemical observations of the conditions under which arc magma forms. In general the predicted maximum temperature below arcs is a bit too low to trigger melting in anhydrous peridotite but the addition of fluids, that lower the dry solidus by a relatively small amount, appear sufficient to explain flux melting (Figure 3). Even with these small shifts the solidus remains well above the peridotite dehydration solidus which would trigger more extensive melting (e.g., Turner et al., 2012).

Figure 3 Below-arc temperatures and melting potential in the Alaska subduction zone. The dry solidus for peridotite indicated by "H" (Hirschmann, 2000) requires minor shifting in temperature to produce a source for primary magmas. "H-30" and "H-80" indicate shifts by 30 and 80°C, respectively. This is the range between which magmas are created that generate on average 4 wt% H_2O which is the global average (Plank et al., 2013). a) Thermal model for Alaska (similar to that in Syracuse et al., 2010) with regions that would experience melt if the dry solidus would be shifted by 30 and 80°C. The triangle marks the location of the volcanic front at this cross-section. b) Temperature below the arc and intersection with the shifted dry peridotite solidus.

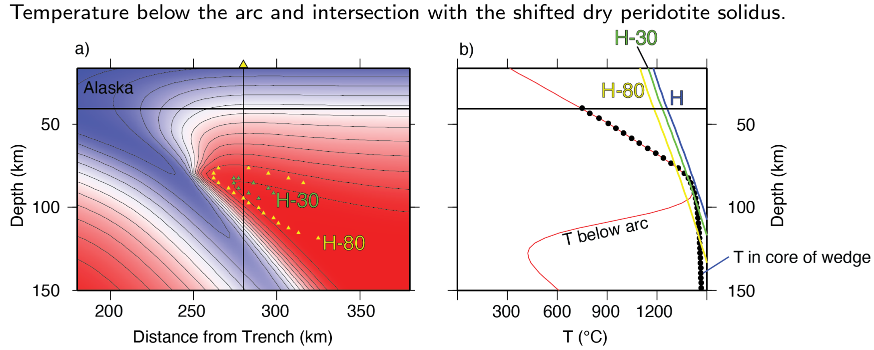

The thermal models tend to have a somewhat thick overriding lithosphere causing the zone of primary melt formation to be relatively deep below the volcanic arc. While this is consistent with seismological and geochemical constraints for some regions (e.g., Hopkins et al., 2020) it has been frequently pointed out that the primary arc magmas tend to be last equilibrated at lower pressures than is predicted by the thermal models. For example, Baziotis et al. (2018) reported that primary melt formation below Santorini, Greece is by flux melting at 1323°C and 1.7 GPa (or about 60 km) with similar conditions reported for magma generation below the Colima Graben, Mexico (Becerra-Torres et al., 2020). Global compilations constrain the hottest part of the shallow wedge from P-T conditions of last melt equilibration between 1100–1400°C at 1–1.7 GPa (Grove et al., 2012; Kelemen et al., 2003; Till, 2017). In other words, while the thermal models tend to have high enough temperatures below the arc, the depth of the maximum temperature is 30–40 km too deep compared to geochemical and petrological constraints. It remains a question whether these differences could be explained by advection of heat by ascending magma (e.g., Melekhova et al., 2015; Rees Jones et al., 2018) or that significant thinning of the lithosphere below the arc accompanied by asthenospheric flow is required. While thermal models providing such asthenospheric flow have been constructed (Kelemen et al., 2003) or sketched (England and Katz, 2010; Perrin et al., 2016), we are not aware of any published work that fully integrates these petrological constraints with magma transport modeling and geophysical constraints.

3.3 Geophysical imaging of metamorphic reactions

Subduction zone thermal models can be combined with thermodynamic modeling to predict where major dehydration reactions can occur (Hacker et al., 2003; van Keken et al., 2011) which then in turn can be compared to observations. Various geophysical techniques have been used to demonstrate changes in seismic or electromagnetic properties of the subducting slab that suggest major metamorphic changes, including dehydration and the corresponding production of fluids, that tend to correlate well with the predictions of such metamorphic reactions from recent thermal subduction zone modeling. Receiver function studies, which use conversions of seismic waves to locate seismic velocity interfaces, have successfully been used to map out subduction zone metamorphism. One example is in Rondenay et al. (2008) that clearly shows a low seismic velocity layer where hydrated oceanic crust is expected in both Central Alaska and Cascadia, with the crucial difference that this low velocity layer disappears at much shallower depth in Cascadia than in Central Alaska. This is predicted by thermal modeling with a resulting deeper stability of hydrous phases in the colder Central Alaska subduction zone. Updated imaging for the low velocity oceanic crust below Central Alaska using scattered wave energy is in Mann et al. (2022). For Cascadia, the low velocity layer correlates partly with an anomalously high ratio of P- to S-wave velocities, suggesting the presence of free fluids with high pore pressure (Peacock et al., 2011) that coincides with a region of low frequency earthquakes (Calvert et al., 2020).

As discussed in part I, there appears to be a strong thermal-petrological control on the location of intermediate-depth seismicity, with (upper plane) seismicity mostly contained in the oceanic crust in cold subduction zones and earthquakes occurring primarily in the slab mantle in warm subduction zones (Abers et al., 2013). In cold subduction zones such as NE Japan the seismicity appears to be limited by the transformation of the oceanic crust from blueschist facies to lawsonite-eclogite facies conditions (see Figure 3 in part I). The blueschist breakdown and transition of lawsonite eclogite to anhydrous eclogite in NE Japan is also imaged as an increase in P-wave velocity in a study using multi-pathing of high frequency waves (Wu and Irving, 2018). The Central Alaska subduction zone is another example of a relatively cold subduction zone where intermediate-depth earthquakes occur in the crust and tend to deepen into the crust before disappearing near the slab Moho at ∼120–130 km depth (Rondenay et al., 2008). Thermal modeling suggests again a key role for the “blueschist-out” dehydration boundary here (Abers et al., 2013, see also part I). In this case earthquakes are seen to step down along a linear trend through the crust with depth (see Figure 2 in Abers et al., 2013). This suggests the earthquakes may line up with the dehydration boundary and this could therefore be one rare location that might suggest dehydration embrittlement is responsible for intermediate-depth seismicity (see discussion in part I).

It also appears possible to see the disappearance of lawsonite eclogite from measurements of electrical conductivity. For example, Manthilake et al. (2015) showed that the high conductivity region in NE Japan and Chile could be explained by the updip presence of highly conductive fluids released by lawsonite dehydration occurring at depths predicted by thermal modeling. A similar conclusion can be drawn for Cascadia, but now for shallow fluids released by the basalt-eclogite transition at ∼50 km depth (Pommier et al., 2019; Wannamaker et al., 2014).

3.4 Comparison to the exhumed rock record

Insights into the thermal structure of past subduction zones are provided by the study of blueschists and eclogites that are exhumed from such subduction zones. These can be analyzed for the pressure-temperature(-time) paths they experienced during subduction and exhumation. Peak metamorphic pressure-temperature conditions determined from such exhumed rocks generally fall within the high-pressure domain before the quartz-coesite phase boundary at around 2.5 GPa. This corresponds quite well with the decoupling depth of 75–80 km suggesting that any oceanic crust that reaches this depth is permanently subducted past this “point of no return” (Whitney et al., 2014).

In some cases reasonable agreement is found between prograde P-T paths in certain localities and conditions predicted by related thermal modeling. See, for example, compilations and comparisons for the Alps in Bebout et al. (2013) and Debret et al. (2021). Scambelluri et al. (2016) studied the fluid-rock evolution of marble and carbonated serpentinite in the Ligurian Alps (Italy) and estimated P-T conditions at around 550°C at 2.4 GPa. Fluid-related inclusions in peridotite from the Swiss Alps were used to estimate a much higher temperature range of 800–850°C at 3 GPa (Scambelluri et al., 2015). Both fall within the global range of temperature predictions in Syracuse et al. (2010) Combined these observations could reflect the rapid temperature increase of the slab surface near the coupling point. Interpreted P-T conditions from blueschist units on Sifnos and Syros (Greece) also show rapid isobaric heating similar to those suggested in the thermal models (Dragovic et al., 2015; Gorce et al., 2021). Relatively rapid heating starting below 3 GPa was also observed by phase equilibrium modeling of a coesite eclogite in the Eastern China Sulu Belt (Xia et al., 2018). A study of lawsonite-eclogite terranes in Alpine Corsica (France) suggested fluids released from deep dehydration reactions traveled along a cool slab P-T path (Piccoli et al., 2018) consistent with some of the coldest models in Syracuse et al. (2010).

When global databases for exhumed rocks from oceanic subduction settings (e.g., Agard et al., 2009, 2018; Brown and Johnson, 2019; Hacker, 1996; Penniston-Dorland et al., 2015; Tsujimori et al., 2006; Whitney et al., 2020) are compared to the global spread of predicted temperatures in the subducting oceanic crust in present-day subduction zones (e.g., Gerya et al., 2002; Syracuse et al., 2010) there appears to be a bigger discrepancy: the rock record provides an average temperature below the forearc that is higher by 100–200°C, and at some depths even up to 300°C, than the predicted average of the thermal models (Penniston-Dorland et al., 2015). In addition, the temperature range predicted for the downgoing oceanic crust in a significant number of subduction zones, that are characterized by fast convergence of old oceanic lithosphere, is not represented in the rock record, except for rare exceptions (Piccoli et al., 2018). These discrepancies have led to the suggestion that the thermal models somehow miss important heat sources (Penniston-Dorland et al., 2015).

Shear heating (that is, the release of energy through frictional processes, such as those occurring by large earthquakes along the seismogenic zone) is one such proposed heat source (e.g., Ishii and Wallis, 2020; van den Beukel and Wortel, 1987). In general, shear heating has been a long-time favorite ad-hoc explanation to explain observations or inferences of thermal conditions in subduction zones that are higher than what might be expected. After all, at first blush it might be difficult to explain the presence of arc volcanoes in an environment that should be cooler than average mantle by the insertion of cold oceanic lithosphere! While early suggestions that shear heating would be responsible for, e.g., the formation of arc volcanoes (Bodri and Bodri, 1978) or the melting of hydrated oceanic crust (Peacock et al., 1994), it has become clear that these processes can be adequately explained by, in turn, hot mantle wedge circulation with related liberation of fluids from the subducting slab leading to flux melting (Gill, 1981) and slab surface temperatures that reach well above the hydrous solidus (van Keken et al., 2002) – see also the discussion in van Keken et al. (2018). It should be noted that the model implementation of shear heating has not always been consistent with basic geophysical, rheological, or mathematical constraints – see examples and discussion in van Keken et al. (2019) and Abers et al. (2020). It also has not been fully realized that the impact of shear heating is rather skin deep, that is, the heating may be efficient to increase temperatures right at the narrow fault zone but heating of the surroundings, and particularly that of the underlying slab crust, is inefficient (see Figure 3C in Molnar and England (1990) and Figure 3 in van Keken et al. (2019)).

As a specific illustration of the lack of depth penetration of shear heating into the slab, we reproduced a model very similar to one in Ishii and Wallis (2020) that was created to mimic the conditions under which rocks were buried (assuming a subduction environment with estimated convergence velocity of 24 cm/yr and incoming lithospheric age of 60 Myr) that were later exhumed in the Sanbagawa belt in SW Japan. We followed their modeling description closely including that of the shear heating along the plate interface, and the assumed subduction zone geometry (Ishii and Wallis, 2020, their Figure 1). We use the shear heating implementation described in Abers et al. (2020) but with the constitutive equations as in Ishii and Wallis (2020, their equations (1)–(4)). The thermal models obtained with Sepran are provided in the Supplementary Information. Given the high thermal parameter the slab is very cold without shear heating (see the black curve in Figure 4a). Adding a large amount of shear heating by increasing the effective friction coefficient μ'

to rather high values (see discussion in Gao and Wang, 2017) allows for the slab surface to reach the observed peak P-T metamorphic conditions (Figure 4a). Note that even with high shear heating at the slab top, the high convergence velocity causes the slab interior to remain rather cold (Figure 4b). The Moho temperature is only modestly affected due to the time it takes for the heat from the top of the slab to diffuse into the crust. Even just 400 m below the slab surface (taken as the top of the sediments) the temperature barely reaches observed P-T conditions. Of course, there could be the happenstance that exhumed rocks are transported to the overriding plate only from the very top of the slab before exhumation via the "subduction channel" (Cloos and Shreve, 1988) or other processes, while rocks deeper in the stratigraphy remain part of the subducting slab and are therefore not represented in the metamorphic rock record.

Figure 4 a) Reproduction of a model by Ishii and Wallis (2020) for the subduction environment thought to be responsible for the burial of rocks later exhumed in the Sanbagawa belt. With high shear heating (controlled by the effective friction coefficient μ') the top of the slab reaches observed maximum P-T conditions indicated by the gray triangle. b) The heating of the slab below the shear zone by thermal diffusion is inefficient. Even a short distance from the top of the slab where the heating occurs the temperature falls below the observed conditions. Model temperatures shown in solid lines is for μ'=0.2. For comparison we plot the Moho temperature of the case without shear heating as well.

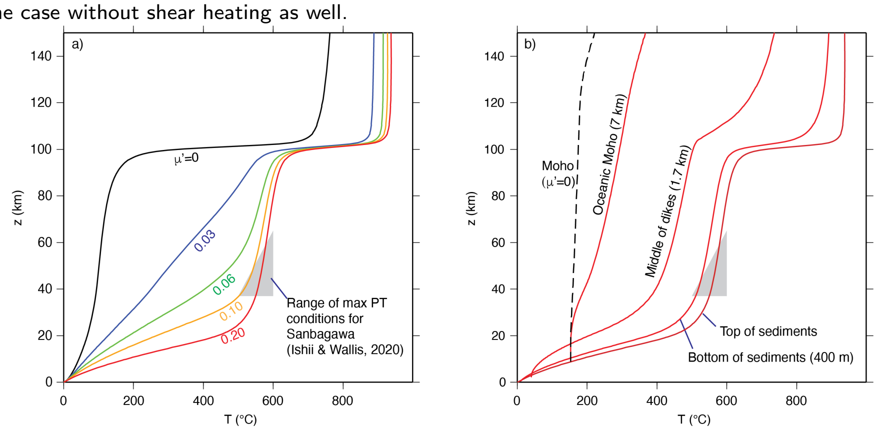

As an alternative explanation for the rock-models discrepancy it has been proposed that the exhumation of rocks is rare and that they may likely sample snapshots of a subduction zone thermal evolution that are warmer on average than the conditions in present day subduction zones (van Keken et al., 2018; Wang et al., 2023). Suggestions that exhumation of rocks occurs with some regularity during subduction initiation and termination provides geological support for this explanation (Agard et al., 2009). Preservation bias is also thought to exist in the Alps with a geological history favoring slow-spreading and small ocean basins with super-extended margins (Agard, 2021). Such oceanic lithosphere would cause elevated temperatures at depth upon subduction compared to that occurring when old oceanic lithosphere is subducted.

It is also entirely possible that these global comparisons between the rock record and thermal models of mature present-day subduction zones are of the proverbial apples vs. oranges type. Future work should benefit significantly from targeted studies where the best paleogeographic constraints with uncertainties on the subduction environment that rocks experienced before exhumation are used. Optimally this includes modeling that takes into account the transfer of the rocks to the overriding plate with subsequent exhumation (e.g., Agard et al., 2018; Ruh et al., 2015). The formation of serpentinite-dominated tectonic mélanges may be favored in warm subduction zones due to the increased dehydration of the subducting slab – this in itself could aid the preferential exhumation of blueschists and eclogites through entrainment in the buoyant rise of less dense serpentinites (Guillot et al., 2015).

Figure 5 Updated comparison between maximum metamorphic P-T conditions determined from exhumed eclogites and blueschists (Whitney et al., 2020) and the current D80 models. Solid lines show slab top temperatures for the coldest oceanic subduction zone (Tonga), one of the coldest continental subduction zones (Tohoku), and two of the warmest subduction zones (Cascadia and Mexico). Lawsonite eclogite data is denoted by the green symbols and lawsonite blueschists in solid blue. Open small circles are from the data base of Penniston-Dorland et al. (2015) with minor modifications as discussed in Whitney et al. (2020) and as made available in their supplementary Table S4. The quartz-coesite (Qz-Coe) and lawsonite-out (Law-out) transitions are shown for reference.

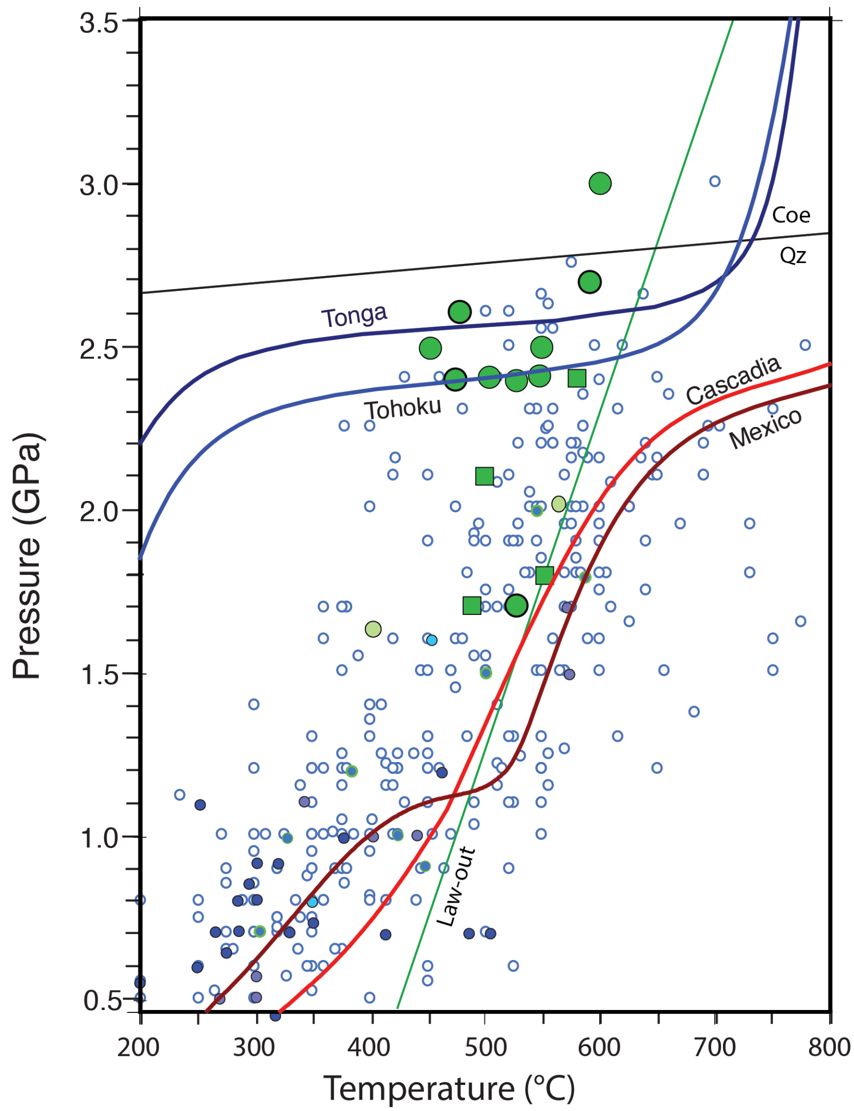

We finish this section with the note that, as discussed above, the corrections to the D80 models make the slab top temperatures slightly warmer than in the original compilation (Syracuse et al., 2010), yet this is not a sufficient shift to help explain the differences with the rock record. For example, Penniston-Dorland et al. (2015) already used the error-corrected and slightly warmer D80 thermal models in their comparison. Figure 5 provides a second example of this – it is an update showing the range of global models with two of the coldest (Tonga and Tohoku) and warmest (Cascadia and Mexico) subduction settings along with a recent global compilation of lawsonite eclogites and lawsonite blueschists (Whitney et al., 2020) and a slightly updated version of the data base of Penniston-Dorland et al. (2015) as discussed in Whitney et al. (2020). The lawsonite eclogite data and a significant proportion of the blueschist data fall within the range of global models, but the near-steady-state models cannot explain the warmest exhumed rock data. The old and fast subduction zones in D80 or D80new still predict rather low temperatures at pressures below 2.5 GPa that in general have not been observed in the rock record. We will offer a partial solution to this dilemma in the discussion about time-dependent and dynamical modeling below.

3.5 H_2O release

We wrap up this section with a less precise but nevertheless important discussion on the role thermal modeling plays in estimating the global water flux and how these estimates can be compared to other models and observations.

Deep transport of water past the arc was predicted by van Keken et al. (2011) to be approximately one third of the bound water that enters the trench or about 3.4×10^8 Tg/Myr. This recycling rate translates to about one ocean mass over the age of the Earth. This result was confirmed, with a similar approach, by Cerpa et al. (2022). Uncertainties in these estimates are incurred by the assumed relative proportion of serpentinization and the thickness of the serpentinite layer in the uppermost mantle of the subducting slab.

Wada et al. (2012) showed that localized hydration (compared to the uniform hydration assumed in the previous studies) should lead to greater fluid release from the slab and consequently a smaller global flux to the deep mantle. By contrast, a model study assuming a much larger extent of upper mantle hydration that also employed a parameterization of water input as a function of subduction speed, lithosphere age, and mantle potential temperature suggested nearly double the water transport to the deep mantle and demonstrated water transport may still be efficient, if to a lesser extent, in the hotter Archean (Magni et al., 2014). It should be noted that model estimates for past water recycling should also take into account petrological changes in the composition of the subducting lithosphere when it is formed from a hotter Archean mantle. Palin and White (2015), for example, showed that the Archean lithosphere could contain more water on average and that deep water recycling could therefore have been more efficient.

Parai and Mukhopadhyay (2012) used a Monte Carlo modeling approach to estimate the global water fluxes constrained by a combination of observations that included magma production rate, water content in primary magmas, and sea-level change. They argued for a smaller budget of water input into subduction zones than had been previously assumed (e.g., Rüpke et al., 2004; Schmidt and Poli, 1998). The authors of the present paper find it remarkable that in Figure 4 of Parai and Mukhopadhyay (2012), the water flux estimate from van Keken et al. (2011) meets the band of Monte Carlo models with the highest success rate of fitting the observations where it corresponds to an average arc magma H_2O content of 4 wt%. This arc magma water content has been argued to be a global average in independent work (Plank et al., 2013). Future work may confirm whether the alignment suggested between the results presented in van Keken et al. (2011), Parai and Mukhopadhyay (2012), and Plank et al. (2013) are indications of close agreement between model results and geochemical observations or that they merely represents a fortunate coincidence.

4 Discussion

The thermal models we discussed in detail above either assume a steady-state heat equation (Wada and Wang, 2009) or integrate the time-dependent set of equations for sufficiently long geologic time for the slab thermal structure in the slab to become quasi steady state (Syracuse et al., 2010). As a reminder, important limiting assumptions also include i) a particular isotropic temperature- and strain-rate-dependent creep law for the mantle; ii) a kinematically prescribed slab surface, iii) the assumption of 2D models; iv) solid-state advection without magma or fluid transport; v) a rigid and relatively thick overriding lithosphere; and vi) near constancy of various parameters (such as thermal conductivity and heat capacity that are modeled independent of temperature) in the constitutive equations. While a full discussion of the impact of these assumptions is beyond the scope of this manuscript, we will briefly address work that has used more realistic subduction zone model assumptions.

Time-dependent modeling The assumption of near steady state might be appropriate when studying the slab thermal structure in mature subduction zones that have near-constant geometry and forcing parameters (such as, say, Tohoku, but certainly not Nankai – see discussion in part I). Other cases where one needs to consider time-dependent processes is during the incipient stages of subduction (Maunder et al., 2020; Soret et al., 2022) or during the final stages of the evolution of a subduction zone including slab break off (Freeburn et al., 2017) and continental subduction (Luo and Leng, 2021). In addition to the considerations for exhumed rocks as discussed in section 3.4, Lee and King (2010) and Kim and Lee (2014) suggest the importance of early thermal evolution of subduction zones in the formation of adakites and boninites.

Backarc spreading A number of the world's subduction zones (such as the Marianas and Tonga) are characterized by moderate to strong backarc spreading which leads to a modification of the lithospheric structure through thinning. This in itself may help explain the divergence between our model predictions for melting below arcs and petrological constraints as discussed in section 3.2. It may also lead to decompression melting similar to that occurring below mid-oceanic ridges (e.g., Kincaid and Hall, 2003). It has also been noted that small-scale circulation in backarc regions, even without extension, can lead to significantly elevated temperatures at relatively shallow depth (Currie and Hyndman, 2006). In an interdisciplinary study, Hall et al. (2012) studied the importance of backarc spreading on the gradual melt depletion of the mantle wedge and the subsequent temporal evolution of arc volcanism. Ishii and Wallis (2022) recently suggested a connection between the slab interacting with the mantle transition zone and cyclic evolution of backarc spreading observed at Tonga and the Marianas. A more global comparison quantifying the type of episodicity of backarc spreading was provided by Clark et al. (2008).

3D geometries A major advantage of the use of 2D modeling is computational efficiency. The extension to 3D, particularly when considering time-dependence, tends to be very expensive when sufficient spatial and temporal resolution is used. The use of 2D cross-sections may be appropriate for subduction zones that have modest trench-parallel changes in geometry, overriding plate structure, and driving factors such as the age of the incoming lithosphere and convergence speed. In most other cases 3D geometries need to be considered. As an example, Wada et al. (2015) showed that 2D model cross-sections were appropriate for the Tohoku subduction zone, but that 3D modeling should be used at Hokkaido due to the oblique convergence there and that this better explained observations of intermediate-depth seismicity and location of arc volcanoes. Even in steady state, 3D models with along-arc variation show significant trench-parallel and/or toroidal flow (Bengtson and van Keken, 2012; Kneller and van Keken, 2007, 2008) which is important for understanding of seismic anisotropy and geochemical signatures (as discussed in section 3.1). Oblique convergence can cause temperature differences of several hundred degrees Celsius as demonstrated in models with isoviscous (Plunder et al., 2018) and temperature-dependent wedge rheology (Bengtson and van Keken, 2012). A number of subduction zones such as Nankai and Mexico have further complications of potential slab tears and folds which makes the model design increasingly difficult – a recent study using advanced visualization suggested slab windows and other discontinuous features might be more important globally than had hitherto been realized (Jadamec et al., 2018).

Dynamical subduction zone models The assumption of a kinematic slab (or at least a kinematically driven slab surface) is very useful when modeling specific subduction zones that have clear slab geometries and known driving forces but becomes limiting when trying to understand the dynamics of subduction zones. Such dynamical models (e.g., Holt and Condit, 2021; Kincaid and Sacks, 1997) may be particularly important when considering the exhumation of blueschists and eclogites. For such studies it might be essential to take into account buoyancy forces other than that caused by thermal expansion. Simple density arguments would suggest eclogites need to be exhumed by buoyant transfer in either sediments or serpentinized rock as quantitatively demonstrated by, for example, Wang et al. (2019). We also note the importance of hybrid kinematic-dynamic models that explore the dynamics of the mantle wedge and overriding lithosphere as driven by chemical and thermal buoyancy forces with highly variable rheologies (see e.g., Gerya, 2011).

Dynamical models have the potential to provide important new perspectives on the thermal structure of subduction zones at least in a generic sense since slabs are,

Figure 6 a) Modified from Holt and Condit (2021, their Figure 3a). Solid lines show the temperature evolution at the top of the slab in a fully dynamic model of subduction initiation below a young oceanic lithosphere (see their Figure 2). As time progresses the slab top cools and adjusts to a near-steady-state thermal structure after ∼20 Myr that is reminiscent of the near-steady-state ones discussed in this paper. A18=Agard et al. (2018) with t' their estimate whether rocks were subducted during subduction initiation (t'=0), termination (t'=1), or some time in between. Symbols become larger with duration of subduction. SPD15p: prograde paths from Penniston-Dorland et al. (2015) as used in van Keken et al. (2018). HC21 indicates the slab paths from Holt and Condit (2021) with three paths highlighted with age. b)-d) Slab paths from D80 shown every 1 Myr for 15 Myr in red for three subduction zones. Black line is the near-steady-state top of slab temperature (after 20 Myr for ocean-ocean settings and 40 Myr for ocean-continent ones). b) Top of slab thermal evolution in a subduction zone where the slab sinks below a young oceanic lithosphere, as assumed in Holt and Condit (2021) with a similar slab temperature evolution as in a). c) Thermal evolution of the slab top below Colombia Ecuador characterized by moderately fast convergence in an ocean-continent setting with relatively large dip. d) Thermal evolution predicted for Central Honshu characterized by fast ocean-continent subduction with an old incoming plate. Note that in all frames we only show the slab paths to the pressure corresponding to the depth that the slab tip has reached.

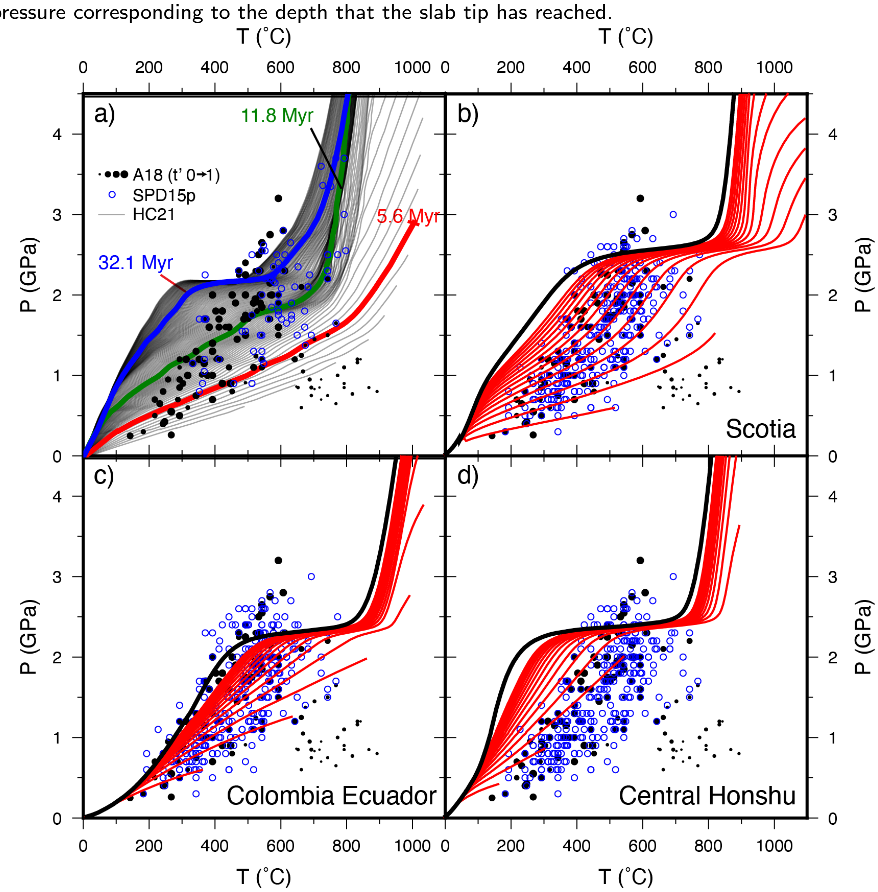

of course, dynamic entities. A full comparison between the thermal structure predicted by dynamical models and the kinematic-dynamic models used here is beyond the scope of this manuscript. Such a comparison is also made difficult by the paucity of reported slab surface temperatures or other constraints on the thermal structure that can be directly compared to the kinematic-dynamic models or geophysical and geochemical observations. Any such comparisons are further complicated by the dynamic nature of slabs, where the slab deforms, rolls back (or advances), and can have a widely variable age of the lithosphere at the trench and convergence velocity. For example, in the model presented by Holt and Condit (2021) the convergence speed is slow at the start (<2 cm/yr), ramps up within about 10 Myr to 12 cm/yr, and then reaches a near steady state value of about 3 cm/yr after 20 Myr. By design it is much more difficult for such dynamical models to have similar time-dependent evolution as those constrained for various subduction zones from paleogeographic constraints on plate speed and lithospheric ages (see, e.g., Coltice et al., 2013).

Figure 6 provides a simple comparison of the consequences of using such a dynamical model vs. our kinematic-dynamic models on the slab surface temperature. Note that we only show the slab temperature paths to the pressure corresponding to the depth to which the slab tip has progressed. The predicted slab top temperatures from the dynamic model reach high temperatures early due to the assumption of a very thin overriding lithosphere. The models shown in Figure 6b are for our D80 Scotia model which is also characterized by convergence below an overriding plate with young oceanic lithosphere. The focus on subduction initiation below a thin lithosphere might be appropriate given that subduction appears to initiate in ocean-ocean settings or in ones where the overriding continental crust has been thinned significantly (e.g., Agard, 2021; Crameri et al., 2020). Some ocean-continent convergence zones also match the metamorphic rock record initially provided subduction is sufficiently fast and the slab geometry has a sufficiently high initial dip, as is the case for Colombia Ecuador (Figure 6c). A number of models that initiate below a continental overriding plate see cooler conditions in their initial evolution particularly in the case of old slabs with low initial dip (see Figure 6d and the full compilation provided in the Supplementary Information). Just under one third of the D80 models show slab paths that correspond to the eclogite and blueschist data (see Supplementary Information).

Clearly the thermal environment during subduction initiation under certain conditions is predicted to be significantly warmer at shallow pressures compared to that for mature subduction zones with a gradual rotation of the geothermal gradient from very high to modest and then rather low values. Except for the final stages, the rotation of the geothermal gradient is similar to that suggested from the geologic record with metamorphic soles forming before high-temperature and then low-temperature eclogites (see e.g., Agard et al., 2020, their Figure 16). Note that the metamorphic sole conditions are not quite reached by any of the models presented in Figure 6 and that there is only one that does in the full D80 compilation (New Britain, which is characterized by fast convergence below a young overriding lithosphere – see Supplementary Information). The formation of these metamorphic soles might require subduction initiation under different conditions than modeled here (see e.g., discussion and models in Zhou and Wada, 2021).

As discussed in Billen and Arrendondo (2018), some published dynamical models (e.g., Garel et al., 2014; Čížková and Bina, 2013) develop rather cold mantle wedges suggesting low below-arc slab surface temperatures that are inconsistent with constraints from geophysics and geochemistry as discussed above. This may partly be due the need for using somewhat lower spatial resolution in these models that often have larger geometries and are intrinsically significantly more computationally expensive than the kinematic-dynamic models, but it could also be due to the treatment of the wedge rheology. Billen and Arrendondo (2018) showed that with a composite dislocation and diffusion creep law (Hirth and Kohlstedt, 2003), that reaches sufficiently low viscosity in the mantle wedge, models develop a thermal structure of the mantle wedge and top of the slab are consistent with observational constraints and within the range of that predicted by our kinematic-dynamic models. Compare, for example, their Figure 6 with our Figure 2 and their Figure 7 with our Figure 3.

Incorporation of fluid & magma generation and flow The generation and transport of fluids and melts in subduction zones may have an important, if possibly localized influence on subduction zone thermal structure and dynamics through advective heat transport and feedback on rheology and other constitutive parameters. It has for example been demonstrated that hydrothermal circulation in the shallow oceanic crust has an important but local advective cooling effect particularly for young oceanic lithosphere (Rotman and Spinelli, 2013; Spinelli et al., 2018). Several models explore the importance of driving forces created by fluid generation and migration (Cerpa et al., 2017; Ha et al., 2020; Wilson et al., 2014) and the relative importance of porous vs. channelized flow (Katz et al., 2022). Disequilibrium fluid transport such as that through channels may affect temperature more strongly than when instantaneous chemical equilibrium processes are assumed (Ikemoto and Iwamori, 2014). Wada and Behn (2015) suggested that large grain size variations along the base of the mantle wedge have an important influence on fluid flow in the wedge and could help focus the fluid flow towards the arc location.

Variations in thermodynamic parameters Effects of variable thermal conductivity, heat capacity, and density tend to be fairly significant at low T and but considerably more modest at higher T. Maierová et al. (2012) reported up to 125°C local differences due to variable conductivity but their predicted overall changes in the subduction zone thermal structure are more subtle. An interesting and more complete extension of this study was in Chemia et al. (2015), who took into account variable thermal properties, phase transformations (including devolatilization reactions) and suggested again that the dominant effect was under low T with variations in subducting sediments and oceanic crust warming by just 40–70°C; an exception was the larger cooling effect seen in fluid-saturated sediments upon subduction. Morishige and Tasaka (2021) extended models of subduction zone thermal structure to include anisotropic conductivity in Tohoku where seismic anisotropy is large – they found the effects of anisotropy was minimal on thermal structure. Similar small effects of variable conductivity, heat capacity, and density on the thermal structure of subduction zones were shown by Guo et al. (2022), Morishige (2022), and van Zelst et al. (2023). Lev and Hager (2011) showed that the use of anisotropic viscosity (which is likely due to the potential for strong fabric production in the mantle wedge flow) also has a modest effect on slab top temperatures (up to just 35°C). We conclude that variations in the constitutive parameters discussed here have a rather modest effect compared to those incurred, say, by changes in the thermal parameter.

5 Conclusions

We have used high resolution finite element modeling to update a global suite of subduction zone models. An intercomparison using two independent finite element approaches shows excellent agreement – a comparison between a selection of these models and a previously published compilation shows reasonable agreement despite significant differences in the assumptions and solution methods. We have shown that, with exceptions, there is in general good, and in some cases remarkable, agreement between model predictions and independent geophysical and geochemical estimates. Significant work can be done in the near future to enhance our understanding of the thermal structure of subduction zones from an interdisciplinary perspective.

Availability of data and material

The petrological data shown in the figures are taken from the literature. The TerraFERMA and Sepran modeling data shown in the figures are provided in the zenodo repository available at doi.org/10.5281/zenodo.7843967. The TF modeling data can be independently reproduced using the input files provided in https://github.com/cianwilson/vankeken_wilson_peps_2023, which can be run using the docker images contained in https://github.com/users/cianwilson/packages/container/package/vankeken_wilson_peps_2023. The zenodo repository contains all files and information listed as Supplemental Information.

Competing interests

The authors declare that they have no competing interest.

Funding

This work was supported in part by National Science Foundation grants 1850634 and 2021027 to PvK.

Authors' contributions

Both authors conceived of the approach to the review paper. CW provided the main modeling using TerraFERMA, PvK provided the Sepran models. Both authors contributed to writing this paper.

Acknowledgements

We thank Ikuko Wada for providing the model results from Wada and Wang (2009). We thank Ellen Syracuse for help providing the minor corrections in Table 2 of Syracuse et al. (2010). We thank Sarah Penniston-Dorland, Philippe Agard, Geoff Abers, Chris Ballentine, Scott King, Donna Whitney, Adam Holt, Cailey Condit, and Jon Blundy for discussion and/or comments on an earlier version of the manuscript. We also thank editor Magali Billen and two anonymous reviewers for many constructive comments & questions that helped us to improve the manuscript.

References

Abers, G.A, van Keken, P.E, Wilson, C.R (2020) Deep decoupling in subduction zones: Observations and temperature limits. Geosphere 16, 1408–1424. doi:10.1130/GES02278.1

Abers, G.A, Nakajima, J, van Keken, P.E, Kita, S, Hacker, B.R (2013) Thermal-petrological controls on the location of earthquakes within subducting plates. Earth Planet Sci Lett 369–370, 178–187. doi:10.1016/j.epsl.2013.03.022

Agard, P (2021) Subduction of oceanic lithosphere in the Alps: Selective and archetypal from (slow-spreading) oceans. Earth-Sci Rev **214**. Art No 103517, doi:10.1016/j.earscirev.2021.103517

Agard, P, Yamato, P, Jolivet, L, Burov, E (2009) Exhumation of oceanic blueschists and eclogites in subduction zones: Timing and mechanisms. Earth-Sci Rev 92, 53–79. doi:10.1016/j.earscirev.2008.11.002

Agard, P, Plunder, A, Angiboust, S, Bonnet, G, Ruh, J (2018) The subduction plate interface: Rock record and mechanical coupling (from long to short timescales). Lithos 320–321, 537–566. doi:10.1016/j.lithos.2018.09.029

Agard, P, Prigent, C, Soret, M, Dubacq, B, Guillot, S, Deldicque, D (2020) Slabitization: Mechanisms controlling subduction development and viscous coupling. Earth-Sci Rev **208**. Art No 103259, doi:10.1016/j.earscirev.2020.103259

Baziotis, I, Kimura, J-I, Pantazidis, A, Klemme, S, Berndt, J, Asimow, P.D (2018) Geophysical source conditions for basaltic lava from Santorini volcano based on geochemical modeling. Lithos 316–317, 295–303. doi:10.1016/j.lithos.2018.07.027

Bebout, G.E, Agard, P, Kobayashi, K, Moriguti, T, Nakamura, E (2013) Devolatilization history and trace element mobility in deeply subducted sedimentary rocks: Evidence from Western Alps HP/UHP suites. Chem Geol 342, 1–20. doi:10.1016/j.chemgeo.2013.01.009

Becerra-Torres, E, Melekhova, E, Blundy, J.D, Brooker, R.A (2020) Experimental evidence for decompression melting of metasomatized mantle beneath Colima Graben, Mexico. Contr Miner Petrol **175**. Art No 101, doi:10.1007/s00410-020-01740-x

Bengtson, A.K, van Keken, P.E (2012) Three-dimensional thermal structure of subduction zones: effects of obliquity and curvature. Solid Earth 3, 365–373. doi:10.5194/se-3-365-2012

Billen, M.I, Arrendondo, K.M (2018) Decoupling of plate-asthenosphere motion caused by non-linear viscosity during slab folding in the transition zone. Phys Earth Planet Inter 281, 17–30. doi:10.1016/j.pepi.2018.04.01

Bodri, L, Bodri, B (1978) Numerical investigation of tectonic flow in island-arc areas. Tectonophysics 50, 163–175. doi:10.1016/0040-1951(78)90133-6

Brown, M, Johnson, T (2019) Metamorphism and the evolution of subduction on Earth. Amer Miner 104, 1065–1082. doi:10.2138/am-2019-6956

Calvert, A.J, Bostock, M.G, Savard, G, Unsworth, M.J (2020) Cascadia low frequency earthquakes at the base of an overpressured subduction shear zone. Nat Comm **11**. Art No 3874, doi:10.1038/s41467-020-17609-3

Caulfield, J, Turner, S, Arculus, R, Dale, C, Jenner, F, Pearce, J, Macpherson, C, Handley, H (2012) Mantle flow, volatiles, slab-surface temperature and melting dynamics in the north Tonga arc - Lau back-arc basin. J Geophys Res: Solid Earth **117**. Art No B11209, doi:10.1029/2012JB0009526

Cerpa, N.G, Arcay, D, Padrón-Navarta, J.A (2022) Sea-level stability over geological time owing to limited deep subduction of hydrated mantle. Nat Geosc 15, 423–428. doi:10.1038/s41561-022-00924-3

Cerpa, N.G, Wada, I, Wilson, C.R (2017) Fluid migration in the mantle wedge: Influence of mineral grain size and mantle compaction. J Geophys Res: Solid Earth 122, 6247–6268. doi:10.1002/2017JB014046

Chemia, Z, Dolejš, D, Steinle-Neumann, G (2015) Thermal effects of variable material properties and metamorphic reactions in a three-component subducting slab. J Geophys Res: Solid Earth 120, 6823–6845. doi:10.1002/2015JB012080

Chen, M, Manea, V.C, Niu, F, Wei, S.S, Kiser, E (2019) Genesis of intermediate-depth and deep intraslab earthquakes beneath Japan constrained by seismic tomography, seismicity, and thermal modeling. Geophys Res Lett 46, 2025–2036. doi:10.1029/2018GC080025

Clark, S.R, Stegman, D, Müller, R.D (2008) Episodicity in back-arc regimes. Phys Earth Planet Inter 171, 265–279. doi:10.1016/j.pepi.2008.04.012

Cloos, M, Shreve, R.L (1988) Subduction-channel mode of prism accretion, melange formation, sediment subduction, and subduction erosion at convergent plate margins: 1. Background and description. Pure Appl Geoph 128, 455–500. doi:10.1007/BF00874548

Coltice, N, Seton, M, Rolf, T, Müller, R.D, Tackley, P.J (2013) Convergence of tectonic reconstructions and mantle convection models for significant fluctuations in sea floor spreading. Earth Planet Sci Lett 383, 92–100. doi:10.1016/j.epsl.2013.09.032

Cooper, L.B, Ruscitto, D.M, Plank, T, Wallace, P.J, Syracuse, E.M, Manning, C.E (2012) Global variations in H_2O/Ce: 1. Slab surface temperatures beneath volcanic arcs. Geochem Geophys Geosys **13**. Art No Q03024, doi:10.1029/2011GC003902

Crameri, F, Magni, V, Domeier, M, Shephard, G.E, Chotalia, K, Cooper, C, Eakin, C.M, Grima, A.G, Gürer, D, Király, Á, Mulyukova, E, Peters, K, Robert, B, Thielman, M (2020) A transdisciplinary and community-driven database to unravel subduction zone initiation. Nat Comm **11**. Art No 3750, doi:10.1038/s41467-020-17522-9

Crosbie, K.J, Abers, G.A, Mann, M.E, Janiszewski, H.A, Creager, K.C, Ulberg, C.W, Moran, S.C (2019) Shear velocity structure from ambient noise and teleseismic surface wave tomography in the Cascades around Mount St. Helens. J Geophys Res: Solid Earth 124, 8358–8375. doi:10.1029/2019JB017836

Currie, C.A, Hyndman, R.D (2006) The thermal structure of subduction zone back arcs. J Geophys Res: Solid Earth **111**. Art No B08404, doi:10.029/2005JB004024

Debret, B, Garrido, C.J, Pons, M-L, Bouilhol, P, Inglis, E, Sánchez-Vizcaíno, V.L, Williams, H (2021) Iron and zinc stable isotope evidence for open-system high-pressure dehydration of antigorite serpentinite in subduction zones. Geochim Cosmochim Acta 296, 210–225. doi:10.1016/j.gca.2020.12.001

Dragovic, B, Baxter, E.F, Caddick, M.J (2015) Pulsed dehydration and garnet growth during subduction revealed by zoned garnet geochronology and thermodynamic modeling, Sifnos, Greece. Earth Planet Sci Lett 413, 111–122. doi:10.1016/j.epsl.2014.12.024

England, P.C, Katz, R.F (2010) Melting above the anhydrous solidus controls the location of volcanic arcs. Nature 467, 700–703. doi:10.1038/nature09417

Freeburn, R, Bouilhol, P, Maunder, B, Magni, V, van Hunen, J (2017) Numerical models of the magmatic processes induced by slab breakoff. Earth Planet Sci Lett 478, 203–213. doi:10.1016/j.epsl.2017.09.008

Freymuth, H, Elliott, T, van Soest, M, Skora, S (2016) Tracing subducted black shales in the Lesser Antilles arc using molybdenum isotope ratios. Geology 44, 987–990. doi:10.1130/G38344

Gao, X, Wang, K (2017) Rheological separation of the megathrust seismogenic zone and episodic tremor and slip. Nature 543, 416–419. doi:10.1038/nature21389

Garel, F, Goes, S, Davies, D.R, Davies, J.H, Kramer, S.C, Wilson, C.R (2014) Interaction of subducted slabs with the mantle transition-zone: A regime diagram from 2-D thermo-mechanical models with a mobile trench and an overriding plate. Geochem Geophys Geosys 15, 1739–1765. doi:10.1002/2014GC005257

Gerya, T (2011) Future directions in subduction modeling. J Geodyn 52, 344–378. doi:10.1016/j.jog.2011.06.005

Gerya, T.V, Stöckhert, B, Perchuk, A.L (2002) Exhumation of high-pressure metamorphic rocks in a subduction channel: a numerical simulation. Tectonics **21**. Art No 1056, doi:10.1029/2002TC001406

Gill, J.B (1981) Orogenic Andesites and Plate Tectonics. Springer, Heidelberg, Germany. doi:10.1007/978-3-642-68012-0

Gorce, J.S, Caddick, M.J, Baxter, E.F, Dragovic, B, Schumacher, J.C, Bodnar, R.J, Kendall, J.F (2021) Insight into the early exhumation of the Cycladic blueschist unit, Syros, Greece: Combined application of zoned garnet geochronology, thermodynamic modeling, and quartz elastic barometry. Geochem Geophys Geosys **22**. Art No e2021GC009716, doi:10.1029/2021GC009716

Grove, T.L, Till, C.B, Krawczynski, M.J (2012) The role of H_2O in subduction zone magmatism. Annu Rev Earth Planet Sci 40, 413–439. doi:10.1146/annurev-earth-042711-105310

Guillot, S, Schwartz, S, Reynard, B, Agard, P, Prigent, C (2015) Tectonic significance of serpentinites. Tectonophysics 646, 1–19. doi:10.1016/j.tecto.2015.01.020

Guo, J, Zhang, R, Wang, D, Zhang, R, Wang, L, Zhang, J, Cai, N, Miao, S (2022) Thermal conductivity and thermal diffusivity of talc at high temperature and pressure with implications for the thermal structure of subduction zones. J Geophys Res: Solid Earth **127**. Art No e2021JB023425, doi:10.1029/2021JB023425

Ha, G, Montési, L.G.J, Zhu, W (2020) Melt focusing along permeability barriers at subduction zones and the location of volcanic arcs. Geochem Geophys Geosys **21**. Art No e2020GC009253, doi:10.1029/2020GC009253

Hacker, B.R (1996) Eclogite formation and the rheology, buoyancy, seismicity and H_2O content of oceanic crust. In: Bebout, G.E, Scholl, D.W, Kirby, S.H, Platt, J.P (eds.) Subduction: Top to Bottom, Geophysical Monograph 96. American Geophysical Union, Washington, DC, USA, pp 337–346. doi:10.1029/GM096

Hacker, B.R, Peacock, S.M, Abers, G.A, Holloway, S.D (2003) Subduction factory 2. Are intermediate-depth earthquakes in subducting slabs linked to metamorphic dehydration reactions? J Geophys Res: Solid Earth **108**. Art No 2030, doi:10.1029/2001JB001129

Hall, P.S, Cooper, L.B, Plank, T (2012) Thermochemical evolution of the sub-arc mantle due to back-arc spreading. J Geophys Res: Solid Earth **117**. Art No B02201, doi:10.1029/2011JB008507

Hermann, J, Spandler, C.J (2008) Sediment melts at sub-arc depths: an experimental study. J Petrol 49, 717–740. doi:10.1093/petrology/egm073

Hirschmann, M.M (2000) Mantle solidus: Experimental constraints and the effects of peridotite composition. Geochem Geophys Geosys **1**. Art No 2000GC000070, doi:10.1029/2000GC000070

Hirth, G, Kohlstedt, D (2003) Rheology of the upper mantle and mantle wedge: A view from the experimentalists. In: Eiler, J (ed.) Inside the Subduction Factory, Geophysical Monograph 138. American Geophysical Union, Washington, DC, USA, pp 83–105. doi:10.1029/GM138

Holt, A.F, Condit, C.B (2021) Slab temperature evolution over the lifetime of a subduction zone. Geochem Geophys Geosys **22**. Art No e2020GC009476, doi:10.1029/2020GC009476

Hopkins, J.L, Smid, E.R, Eccles, J.D, Hayes, J.L, Hayward, B.W, McGee, L.E, van Wijk, K, Wilson, T.M, Cronin, S.J, Leonard, G.S, Lindsay, J.M, Németh, K, Smith, I.E.M (2020) Auckland Volcanic Field magmatism, volcanism, and hazard: a review. New Zealand J Geol Geophys 64, 213–234. doi:10.1080/00288306.2020.1736102

Ikemoto, A, Iwamori, H (2014) Numerical modeling of trace element transportation in subduction zones: implications for geofluid processes. Earth Planet Space **66**. Art No 26, doi:10.1186/1880-5981-66-26

Ishii, K, Wallis, S.R (2020) High- and low-stress subduction zones recognized in the rock record. Earth Planet Sci Lett **531**. Art No 15935, doi:10.1016/j.epsl.2019.115935

Ishii, K, Wallis, S.R (2022) A possible mechanism for spontaneous cyclic back-arc spreading. Prog Earth Planet Sci 9, 27. doi:10.1186/s40645-022-00486-3

Jadamec, M.A, Kreylos, O, Chang, B, Fischer, K.M, Yikilmaz, M.B (2018) A visual survey of global slab geometries with ShowEarthModel and implications for a three-dimensional subduction paradigm. Earth Space Sci **5**. doi:10.1002/2017EA000349

Katz, R.F, Rees Jones, D.W, Rudge, J.F, Keller, T (2022) Physics of melt extraction from the mantle: speed and style. Ann Rev Earth Planet Sci 50, 507–540. doi:10.1146/annurev-earth-032320-083704

Kelemen, P.B, Rilling, J.L, Parmentier, E.M, Mehl, L, Hacker, B.R (2003) Thermal structure due to solid-state flow in the mantle wedge beneath arcs. In: Eiler, J (ed.) Inside the Subduction Factory, Geophysical Monograph 138. American Geophysical Union, Washington, DC, USA, pp 293–311. doi:10.1029/GM138

Kimura, J-I, Stern, R.J, Yoshida, T (2005) Reinitiation of subduction and magmatic responses in SW Japan during Neogene time. GSA Bull 117, 969–986. doi:10.1130/B25565.1

Kincaid, C, Hall, P.S (2003) Role of back arc spreading in circulation and melting at subduction zones. J Geophys Res: Solid Earth **108**. Art No 2240, doi:10.1029/2001JB001174

Kincaid, C, Sacks, I.S (1997) Thermal and dynamical evolution of the upper mantle in subduction zones. J Geophys Res: Solid Earth 102, 12295–12315. doi:10.1029/96JB03553

Kneller, E.A, van Keken, P.E (2007) Trench-parallel flow and seismic anisotropy in the Mariana and Andean subduction systems. Nature 450, 1222–1225. doi:10.1038/nature06429

Kneller, E.A, van Keken, P.E (2008) Effect of three-dimensional slab geometry on deformation in the mantle wedge: Implications for shear wave anisotropy. Geochem Geophys Geosys **9**. Art No Q01003, doi:10.1029/2007GC001677

Konrad-Schmolke, M, Halama, R, Manea, V.C (2016) Slab mantle dehydrates beneath Kamchatka - yet recycles water into the deep mantle. Geochem Geophys Geosys 17, 2987–3007. doi:10.1002/2016GC006335

Lev, E, Hager, B.H (2011) Anisotropic viscosity changes subduction zone thermal structure. Geochem Geophys Geosys **12**. Art No Q04009, doi:10.1029/2010GC003382

Luo, T, Leng, W (2021) Thermal structure of continental subduction zone: high temperature caused by the removal of the preceding oceanic slab. Earth Planet Phys 5, 290–295. doi:10.26464/epp2021027

Magni, V, Bouilhol, P, van Hunen, J (2014) Deep water recycling through time. Geochem Geophys Geosys 15, 4203–4216. doi:10.1002/2014GC005525

Maierová, P, Chust, T, Steinle-Neumann, G, Čadek, O, Čížková, H (2012) The effect of variable thermal diffusivity on kinematic models of subduction. J Geophys Res: Solid Earth **117**. Art No B07202, doi:10.1029/2011JB009119

Mann, M.E, Abers, G.A, Daly, K.A, Christensen, D.H (2022) Subduction of an oceanic plateau across southcentral Alaska: Scattered-wave imaging. J Geophys Res: Solid Earth **127**. Art No e2021JB022697, doi:10.1029/e2021JB022697

Manthilake, G, Mookherjee, M, Bolfan-Casanova, N, Andrault, D (2015) Electrical conductivity of lawsonite and dehydrating fluids at high pressures and temperatures. Geophys Res Lett 42, 7398–7405. doi:10.1002/2015GL068404

Maunder, B, Prytulak, J, Goes, S, Reagan, M (2020) Rapid subduction initiation and magmatism in the Western Pacific driven by internal vertical forces. Nat Comm **11**. Art No 1874, doi:10.1038/s41467-020-15737-4

Melekhova, E, Blundy, J, Robertson, R, Humphreys, M.C.S (2015) Experimental evidence for polybaric differentiation of primitive arc basalt beneath St. Vincent, Lesser Antilles. J Petrol 56, 161–192. doi:10.1093/petrology/egu074

Molnar, P, England, P (1990) Temperature, heat flux, and frictional stress near major thrust faults. J Geophys Res: Solid Earth 95, 4833–4856. doi:10.1029/JB095iB04p04833

Morishige, M (2022) The thermal structure of subduction zones predicted by plate cooling models with variable

thermal properties. Geophys J Int 229, 1490–1502. doi:10.1093/gji/ggac008
Morishige, M, Tasaka, M (2021) Limited impact of anisotropic thermal conductivity in the mantle wedge on the slab temperature in the Tohoku subduction zone, Northeast Japan. Tectonophysics **820**. Art No 229110, doi:10.1016/j.tecto.2021.229110
Nebel, O, Vroon, P.Z, van Westrenen, W, Iizuka, T, Davies, G.R (2011) The effect of sediment recycling in subduction zones of the Hf isotope character of new arc crust, Banda arc, Indonesia. Earth Planet Sci Lett 303, 240–250. doi:10.1016/j.epsl.2010.12.053
Palin, R.M, White, R.W (2015) Emergence of blueschists on Earth linked to secular changes in oceanic crust composition. Nat Geosc 9, 60–64. doi:10.1038/NGEO2605
Parai, R, Mukhopadhyay, S (2012) How large is the subducted water flux? New constraints on mantle regassing rates. Earth Planet Sci Lett 317–318, 396–406. doi:10.1016/j.epsl.2011.11.024
Peacock, S.M, Rushmer, T, Thompson, A.B (1994) Partial melting of subducting oceanic crust. Earth Planet Sci Lett 121, 227–244. doi:10.1016/0012-821X(94)90042-6
Peacock, S.M, Christensen, N.I, Bostock, M.G, Audet, P (2011) High pore pressures and porosity at 35 km depth in the Cascadia subduction zone. Geology 35, 471–474. doi:10.1130/G31649.1
Penniston-Dorland, S.C, Kohn, M.J, Manning, C.E (2015) The global range of subduction zone thermal structures from exhumed blueschists and eclogites: Rocks are hotter than models. Earth Planet Sci Lett 428, 243–254. doi:10.1016/j.epsl.2015.07.031
Perrin, A, Goes, S, Prytulak, J, Davies, D.R, Wilson, C, Kramer, S (2016) Reconciling mantle wedge thermal structure with arc lava thermobarometric determinations in oceanic subduction zones. Geochem Geophys Geosys 17, 4105–4127. doi:10.1002/2016GC006527
Piccoli, F, Vitale Brovarone, A, Ague, J.J (2018) Field and petrological study of metasomatism and high-pressure carbonation from lawsonite eclogite-facies terrains, Alpine Corsica. Lithos 304–307, 16–37. doi:10.1016/j.lithos.2018.01.026
Plank, T, Cooper, L.B, Manning, C.E (2009) Emerging geothermometers for estimating slab surface temperatures. Nat Geosc 2, 611–615. doi:10.1038/ngeo614
Plank, T, Kelley, K.A, Zimmer, M.M, Hauri, E.H, Wallace, P.J (2013) Why do mafic arc magmas contain ∼4 wt% water on average? Earth Planet Sci Lett 364, 168–179. doi:10.1016/j.epsl.2012.11.044
Plunder, A, Thieulot, C, van Hinsbergen, D.J.J (2018) The effect of obliquity on temperature in subduction zones: insights from 3-D modeling. Solid Earth 9, 759–776. doi:10.5194/se-9-759-2018
Pommier, A, Williams, Q, Evans, R.L, Pal, I, Zhang, Z (2019) Electrical investigations of natural lawsonite and application to subduction contexts. J Geophys Res: Solid Earth 124, 1430–1442. doi:10.1029/2018JB016899
Rees Jones, D.W, Katz, R.F, Tian, M, Rudge, J.F (2018) Thermal impact of magmatism in subduction zones. Earth Planet Sci Lett 481, 73–79. doi:10.1016/j.epsl.2017.10.1015
Rondenay, S, Abers, G.A, van Keken, P.E (2008) Seismic imaging of subduction zone metamorphism. Geology 36, 275–278. doi:10.1130/G24112A.1
Rotman, H.M.M, Spinelli, G.A (2013) Global analysis of the effect of fluid flow on subduction zone temperatures. Geochem Geophys Geosys 14, 3268–3281. doi:10.1002/ggge.20205
Ruh, J.B, Le Pourhiet, L, Agard, P, Burov, E, Gerya, T (2015) Tectonic slicing of subducting oceanic crust along plate interfaces: Numerical modeling. Geochem Geophys Geosys 16, 3505–3531. doi:10.1002/2015GC005998
Rüpke, L.H, Phipps Morgan, J, Hort, M, Connolly, J.A.D (2004) Serpentine and the subduction zone water cycle. Earth Planet Sci Lett 223, 17–34. doi:10.1016/j.epsl.2004.04.018
Ruscitto, D.M, Wallace, P.J, Cooper, L.B, Plank, T (2012) Global variations in H_2O/Ce: 2. Relationships to arc magma geochemistry and volatile fluxes. Geochem Geophys Geosys **13**. Art No Q03025, doi:10.1029/2011GC003887
Scambelluri, M, Pettke, T, Cannaò, E (2015) Fluid-related inclusions in Alpine high-pressure peridotite reveal trace element recycling during subduction-zone dehydration of serpentinized mantle (Cima di Gagnone, Swiss Alps). Earth Planet Sci Lett 429, 45–59. doi:10.1016/j.epsl.2015.07.060
Scambelluri, M, Bebout, G.E, Belmonte, D, Gilio, M, Campomenosi, N, Collins, N, Crispini, L (2016) Carbonation of subduction-zone serpentinite (high-pressure ophicarbonate; Ligurian Western Alps) and implications for deep carbon cycling. Earth Planet Sci Lett 441, 155–166. doi:10.1016/j.epsl.2016.02.034
Schmidt, M.W, Poli, S (1998) Experimentally based water budgets for dehydrating slabs and consequences for arc magma generation. Earth Planet Sci Lett 163, 361–379. doi:10.1016/S0012-821X(98)00142-3
Schmidt, M.W, Vielzeuf, D, Auzanneau, E (2004) Melting and dissolution of subducting crust at high pressures: the key role of white mica. Earth Planet Sci Lett 228, 65–84. doi:10.1016/j.epsl.2004.09.020
Skora, S, Blundy, J (2010) High-pressure hydrous phase relations of radiolarian clay and implications for the involvement of subducted sediment in arc magmatism. J Petrol 51, 2211–2243. doi:10.1093/petrology/egq054
Soret, M, Bonnet, G, Agard, P, Larson, K.P, Cottle, J.M, Dubacq, B, Kylander-Clark, A.R.C, Button, M, Rividi, N (2022) Timescales of subduction initiation and evolution of subduction thermal regimes. Earth Planet Sci Lett **584**. Art No 117521, doi:10.1016/j.epsl.2022.117521
Spinelli, G, Wada, I, Wang, K, He, J, Harris, R, Underwood, M (2018) Diagenetic, metamorphic, and hydrogeologic consequences of hydrothermal circulation in subducting crust. Geosphere 14, 2337–2354. doi:10.1130/GES01653.1
Stein, C.A, Stein, S (1992) A model for the global variation in oceanic depth and heat flow with lithospheric age. Nature 359, 123–129. doi:10.1038/359123a0
Syracuse, E.M, Abers, G.A (2006) Global compilation of variations in slab depth beneath arc volcanoes and implications. Geochem Geophys Geosys **7**. Art No Q05107, doi:10.1029/2005GC001045
Syracuse, E.M, van Keken, P.E, Abers, G.A (2010) The global range of subduction zone thermal models. Phys Earth Planet Int 183, 73–90. doi:10.1016/j.pepi.2010.02.004

Till, C.B (2017) A review and update of mantle thermobarometry for primitive arc magmas. Am Min 102, 931–947. doi:10.2138/am-2017-5783

Tsujimori, T, Sisson, V.B, Liou, J.G, Harlow, G.E, Sorensen, S.S (2006) Very-low-temperature record of the subduction process: A review of worldwide lawsonite eclogites. Lithos 92, 609–624. doi:10.1016/j.lithos.2006.03.054

Turner, S, Hawkesworth, C (1998) Using geochemistry to map mantle flow beneath the Lau Basin. Geology 26, 1019–1022. doi:10.1130/0091-7613(1998)026<1019:UGTMMF>2.3.CO;2

Turner, S, Caulfield, J, Turner, M, van Keken, P, Maury, R, Sandiford, M, Prouteau, G (2012) Recent contribution of sediments and fluids to the mantle's volatile budget. Nat Geosc 5, 50–54. doi:10.1038/NGEO1325

van den Beukel, J, Wortel, R (1987) Temperature and shear stresses in the upper part of a subduction zone. Geophys Res Lett 14, 1057–1060. doi:10.1029/GL014i010p01057

van Keken, P.E, Wilson, C.R (2023) An introductory review of the thermal structure of subduction zones: I – motivation and selected examples. Prog Earth Planet Sci **10**. Art No 42, doi:10.1186/s40645-023-00573-z

van Keken, P.E, Kiefer, B, Peacock, S.M (2002) High-resolution models of subduction zones: Implications for mineral dehydration reactions and the transport of water to the deep mantle. Geochem Geophys Geosys **3**. Art No 1056, doi:10.1029/2001GC000256

van Keken, P.E, Hacker, B.R, Syracuse, E.M, Abers, G.A (2011) Subduction factory: 4. Depth-dependent flux of H_2O from subducting slabs worldwide. J Geophys Res: Solid Earth **116**. Art No B01401, doi:10.1029/2010JB007922

van Keken, P.E, Wada, I, Abers, G.A, Hacker, B.R, Wang, K (2018) Mafic high-pressure rocks are preferentially exhumed from warm subduction settings. Geochem Geophys Geosys 19, 2934–2961. doi:10.1029/2018GC007624

van Keken, P.E, Wada, I, Sime, N, Abers, G.A (2019) Thermal structure of the forearc in subduction zones: A comparison of methodologies. Geochem Geophys Geosys 20, 3268–3288. doi:10.1029/2019GC008334

van Zelst, I, Thieulot, C, Craig, T.J (2023) The effect of temperature-dependent material properties on simple thermal models of subduction zones. Solid Earth 14, 683–707. doi:10.5194/se-14-683-2023

Čížková, H, Bina, C.R (2013) Effects of mantle and subduction-interface rheologies on slab stagnation and trench rollback. Earth Planet Sci Lett 379, 95–103. doi:10.1016/j.epsl.2013.08.011

Wada, I, Behn, M.D (2015) Focusing of upward fluid migration between volcanic arcs: Effect of mineral grain size variation in the mantle wedge. Geochem Geophys Geosys 16, 3905–3923. doi:10.1002/2015GC005950

Wada, I, Wang, K (2009) Common depth of slab-mantle decoupling: Reconciling diversity and uniformity of subduction zones. Geochem Geophys Geosys **10**. Art No Q10009, doi:10.1029/2009GC002570

Wada, I, Behn, M.D, Shaw, A.M (2012) Effects of heterogeneous hydration in the incoming plate, slab rehydration, and mantle wedge hydration on slab-derived H_2O flux in subduction zones. Earth Planet Sci Lett 353–354, 60–71. doi:10.1016/j.epsl.2012.07.025

Wada, I, He, J, Hasegawa, A, Nakajima, J (2015) Mantle wedge flow patterns and thermal structure in Northeast Japan: Effects of oblique subduction and 3-D slab geometry. Earth Planet Sci Lett 426, 76–88. doi:10.1006/j.epsl.2015.06.021

Walowski, K.J, Wallace, P.J, Hauri, E.H, Wada, I, Clynne, M.A (2015) Slab melting beneath the Cascade arc driven by dehydration of altered oceanic peridotite. Nat Geosc 8, 404–408. doi:10.1038/ngeo2417

Walowski, K.J, Wallace, P.J, Clynne, M.A, Rasmussen, D.J, Weis, D (2016) Slab melting and magma formation beneath the southern Cascadia arc. Earth Planet Sci Lett 446, 100–112. doi:10.1016/j.epsl.2016.03.044

Wang, Y, Zhang, L-F, Li, Z-H, Li, Q-Y, Bader, T (2019) The exhumation of subducted oceanic-derived eclogites: Insights from phase equilibrium and thermochemical modeling. Tectonics 38, 1764–1797. doi:10.1029/2018TC005349

Wang, Y, Wang, K, He, J, Zhang, L (2023) On unusual conditions for the exhumation of subducted oceanic rocks: How to make rocks hotter than models. Earth Planet Sci Lett **615**. Art No 118213, doi:10.1016/j.epsl.2023.118213

Wannamaker, P.E, Evans, R.L, Bedrosian, P.A, Unsworth, M.J, Maris, V, McGary, R.S (2014) Segmentation of plate coupling, fate of subducting fluids, and modes of arc magmatism in Cascadia, inferred from magnetotelluric resistivity. Geochem Geophys Geosys 15, 4230–4253. doi:10.1002/2014GC005509

White, W, Copeland, P, Gravatt, D.R, Devine, J.D (2017) Geochemistry and geochronology of Grenada and Union islands, Lesser Antilles: The case for mixing between two magma series generated from distinct sources. Geosphere 13, 1359–1391. doi:10.1130/GES01414.1

Whitney, D.L, Teyssier, C, Seaton, N.C.A, Fornash, K.F (2014) Petrofabrics of high-pressure rocks exhumed at the slab-mantle interface from the "point of no return" in a subduction zone (Sivrihisar, Turkey). Tectonics 33, 2315–2341. doi:10.1002/2014TC003677

Whitney, D.L, F, F.K, Kang, P, Ghent, E.D, Martin, L, Okay, A.I, Vitale Brovarone, A (2020) Lawsonite composition and zoning as tracers of subduction processes: A global review. Lithos **370–371**. Art No 105636, doi:10.1016/j.lithos.105636

Wilson, C.R, Spiegelman, M.S, van Keken, P.E, Hacker, B.R (2014) Fluid flow in subduction zones: The role of solid rheology and compaction pressure. Earth Planet Sci Lett 401, 261–274. doi:10.1016/j.epsl.2014.05.052

Wu, W, Irving, J.C.E (2018) Evidence from high frequency seismic waves for the basalt-eclogite transition in the Pacific slab under northeastern Japan. Earth Planet Sci Lett 496, 68–79. doi:10.1016/j.epsl.2018.05.034

Xia, B, Brown, M, Wang, L, Wang, S-J, Piccoli, P (2018) Phase equilibrium modeling of MT-UHP eclogite: a case study of coesite eclogite at Yangkou Bay, Sulu Belt, Eastern China. J Petrol 59, 1253–1280. doi:10.1093/petrology/egu060

Zamboni, D, Gazel, E, Ryan, J.G, Cannatelli, C, Lucchi, F, Atlas, Z.D, Trela, J, Mazza, S.E, De Vivo, B (2016) Contrasting sediment melt and fluid signatures for magma components in the Aeolian Arc: Implications for modeling of subduction systems. Geochem Geophys Geosys 17, 2034–2053. doi:10.1002/2016GC006301

Zhou, X, Wada, I (2021) Differentiating induced versus spontaneous subduction initiation using thermomechanical models and metamorphic soles. Nat Comm **12**. Art No 4632, doi:10.1038/s41467-021-24896-x